VolRAFT: Volumetric Optical Flow Network for Digital Volume Correlation of Synchrotron Radiation-based Micro-CT Images of Bone-Implant Interfaces

Dr. Tak Ming Wong[1,2,*]
Dr. Julian Moosmann[2]
Dr. Berit Zeller-Plumhoff[1]

[1] Imaging and Data Science
Institute of Metallic Biomaterials
[2] X-Ray Imaging with Synchrotron Radiation
Institute of Materials Physics

Helmholtz-Zentrum Hereon

Helmholtz Imaging Conference 2024
14.05.2024

Helmholtz-Zentrum
hereon

Metallic Biomaterial: Bone Implants

Annual medical treatment cost for trauma in US (Billion dollars)

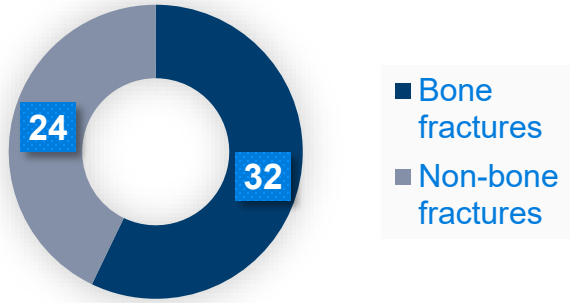

Data from (Tsakiris, 2021)

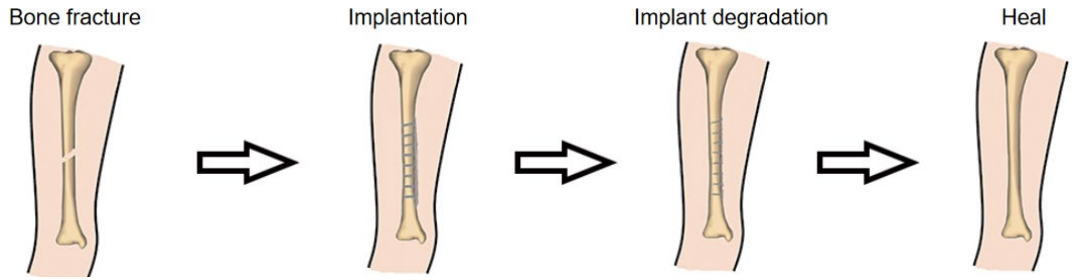

Degradation of the magnesium-based implant in bone fracture healing.
Illustration from (Lu, 2021), used under CC BY 4.0 License.

Bone implants:

- Bone undergoes the most transplants among organs, estimated to be over 3 million surgeries worldwide annually (Tsakiris, 2021)
- Traditional implants (e.g.Titanium):
  - Permanent
  - Need secondary surgery
- Magnesium implants:
  - Bio-degradable
  - Reduce patient's pain, surgery risk and medical cost

Tsakiris, Violeta, Christu Tardei, and Florentina Marilena Clicinschi. "Biodegradable Mg alloys for orthopedic implants–A review." Journal of Magnesium and Alloys 9.6 (2021): 1884-1905.
Lu, Yu, et al. "Biodegradable magnesium alloys for orthopaedic applications." Biomaterials translational 2.3 (2021): 214.

Helmholtz-Zentrum hereon

Metallic Biomaterial: Bio-degradable Mg-Alloy

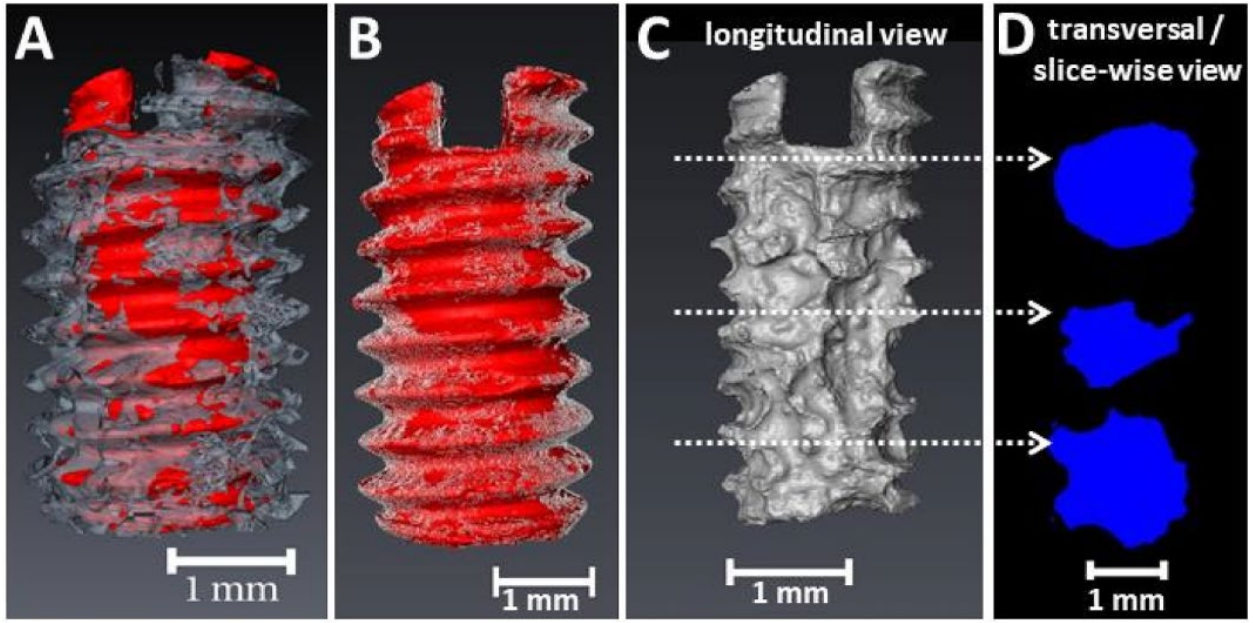

Mg-10Gd implant after 8 weeks in vivo degradation: screw and the surrounding bone (A), the Bone-to-Implant contact (B) and the residual screw (C). Figure from (Krüger, 2021).

Study of degradation:

- Composition of implants
  - How degradation is changed
  - How implant change bone properties
  - Different degradation media
- Mechanical properties of implants
  - Stress and strains
  - Implant stability: push-out/pull-out tests
  - Treatment: heat, extruded, etc.
- Modeling
  - Degradation
  - Composition of degradation layers

Krüger, Diana, et al. "High-resolution ex vivo analysis of the degradation and osseointegration of Mg-xGd implant screws in 3D." Bioactive Materials 13 (2022): 37-52.

Helmholtz-Zentrum hereon

Synchrotron Radiation-based Computed Tomography

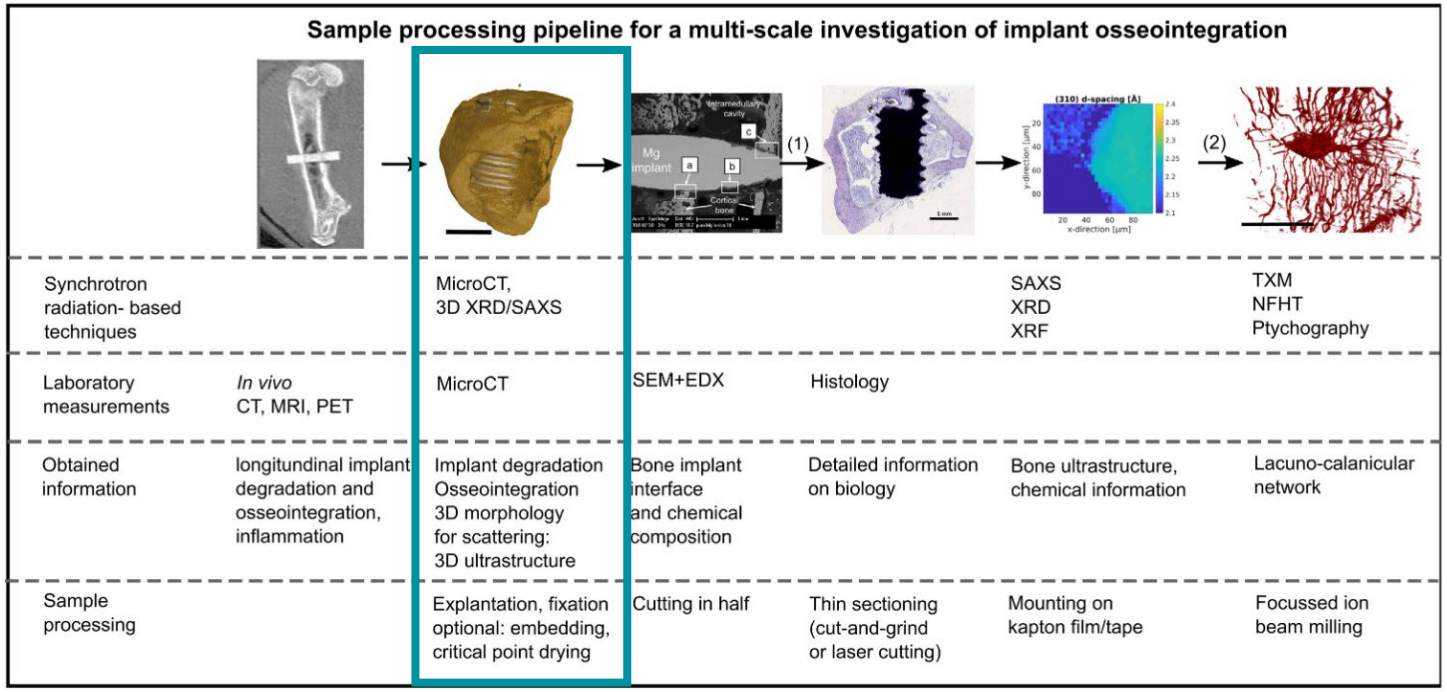

Sample processing pipeline for the multiscale investigation of implant osseointegration covering all hierarchical levels of bone. Figure from (Zeller-Plumhoff, 2021).

Helmholtz-Zentrum Hereon outstation at DESY:

- Operating synchrotron radiation imaging beamlines PETRA III at DESY, Hamburg
- Materials science researches and experiments utilizing X-ray micro-/nano-meters tomography

In situ push-out experiment:

- µCT: voxel size 5.1µm
- Attenuation contrast

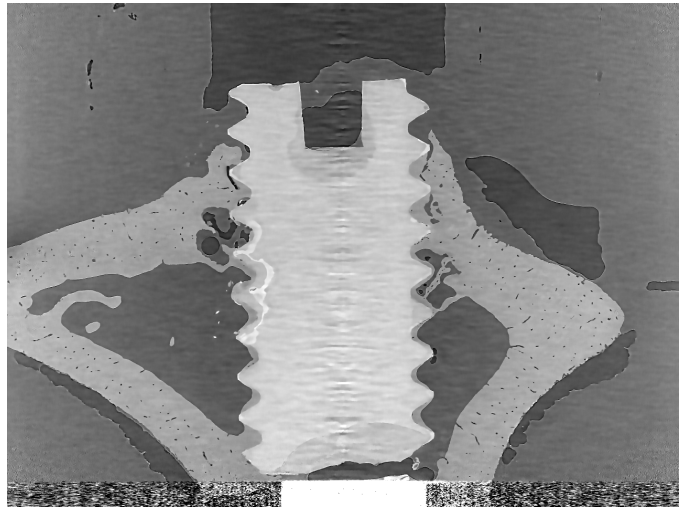

Tomogram of in situ compression of biodegradable bone implant (Bruns, 2023)

Zeller-Plumhoff, Berit, et al. "Utilizing synchrotron radiation for the characterization of biodegradable magnesium alloys—from alloy development to the application as implant material." Advanced Engineering Materials 23.11 (2021): 2100197.
Bruns, Stefan, et al. "On the material dependency of peri-implant morphology and stability in healing bone." Bioactive Materials 28 (2023): 155-166.

Digital Volume Correlation (DVC)

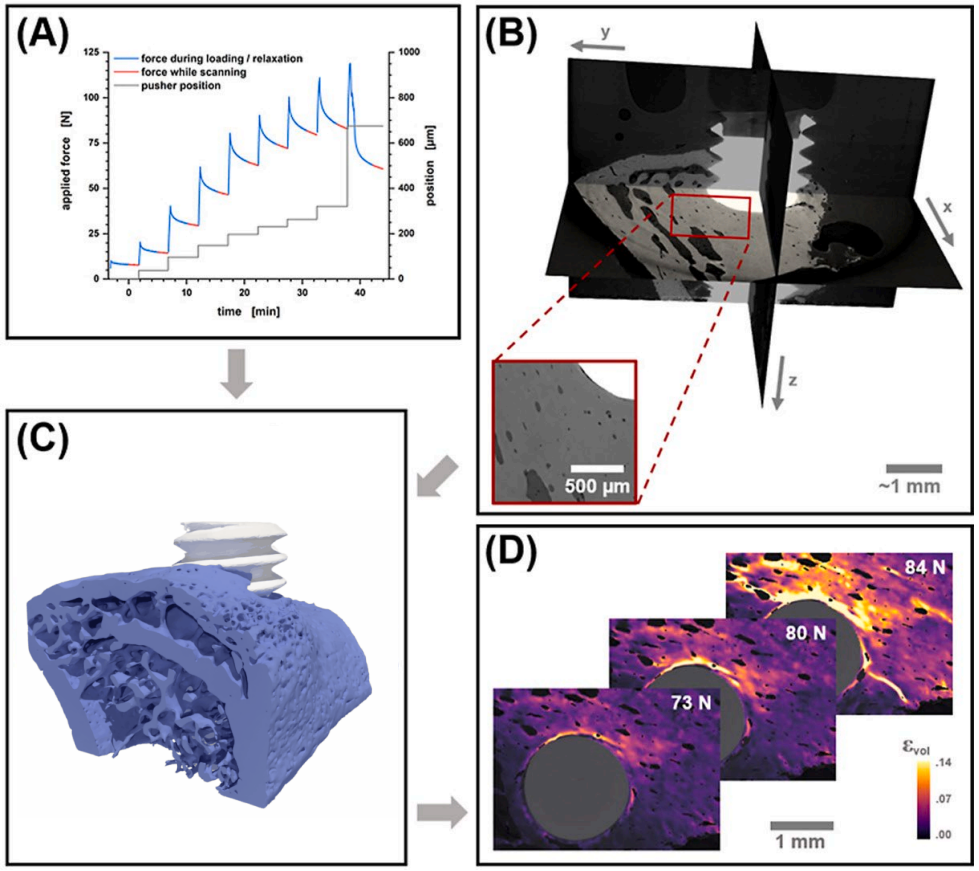

Push-out experiment combined with in situ SRµCT imaging and DVC analysis using an explant with a titanium screw as an example (Bruns, 2023).

Digital Volume Correlation:

- Estimate local volume correlation
- To track bone deformation and strains
- Estimate the 3D displacement field based on the reference (original) volume and the deformed volume

One common technique: Optical flow

- Estimate the displacement (motions) fields of intensities, i.e. *flow field*
- Classical iterative „Knowledge-driven approach“: Hand-crafting of hyperparameters: regularization, image pyramid, filtering, etc.
- Modern ML „data-driven approach“: can outperform by learning the prior knowledge
- Rely heavily on computing powers of GPUs, limited by GPU memory size

Bruns, Stefan, et al. "On the material dependency of peri-implant morphology and stability in healing bone." Bioactive Materials 28 (2023): 155-166.

Helmholtz-Zentrum hereon

VolRAFT: Volumetric Optical Flow Network

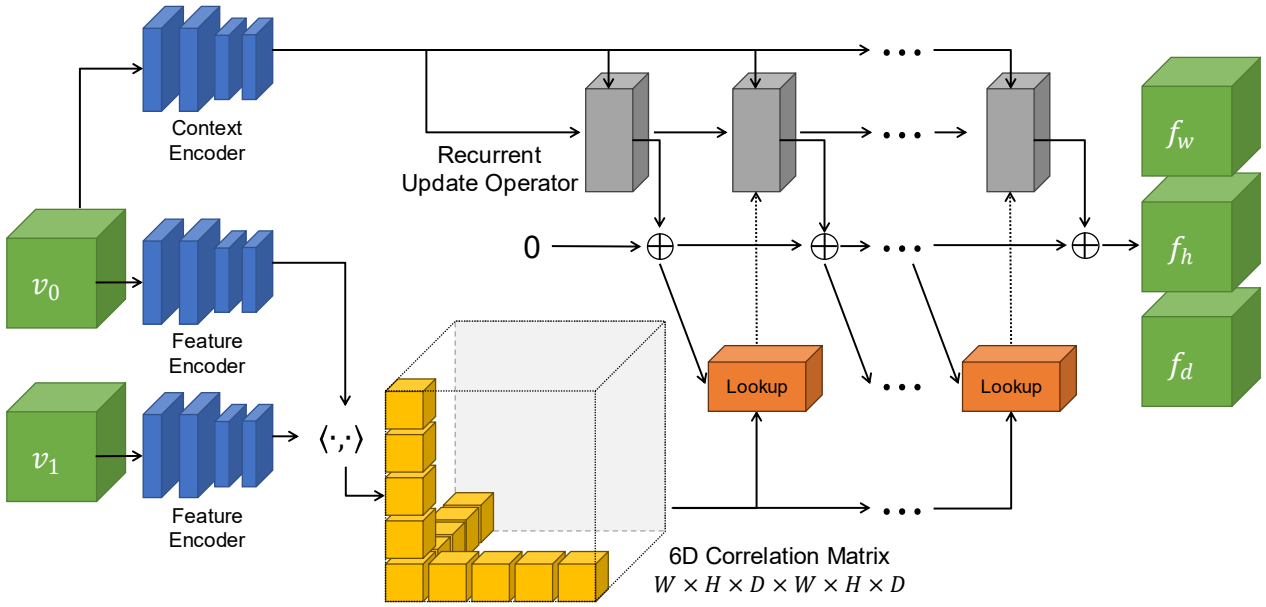

VolRAFT consists of three major parts: feature encoders, a 6D correlation matrix and recurrent 3D update operators.

Contributions:

- Supervised machine learning approach for DVC to estimate 3D displacement fields between 2 volumes.
- Extension of the optical flow network, RAFT (Teed, 2020), from 2D images to 3D volumes.
- Generation of synthetic displacement fields and application to the measured SRµCT volumes for training, validation and testing.
- Comparison to iterative methods [2] for bone-implant loading scenarios based on SRµCT volumes.

Teed, Zachary, and Jia Deng. "RAFT: Recurrent all-pairs field transforms for optical flow." ECCV, 2020.

VolRAFT: Volumetric Optical Flow Network

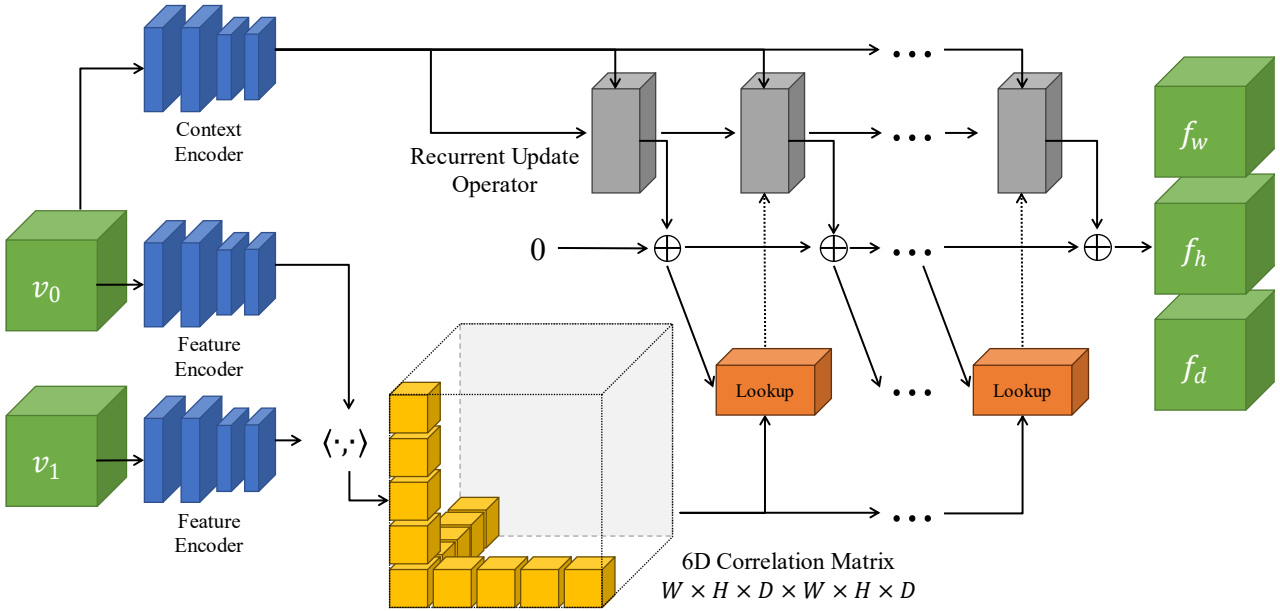

Patch-based approach:

- Splits full volumes (1280 x 1280 x 960) into patches (80 x 80 x 60) for training and inference

Feature/Context encoders:

- Convolutional layers

6D Correlation Matrix:

- Dot product to compute the similarity on multiscale pyramid

Correlation Lookup Operators:

- Generate feature maps by indexing from correlation pyramid

3D Recurrent Update Operators:

- Predict a sequence of displacement field
- Iteratively update

Supervised Loss with a foreground mask:

- Foreground segmentation mask (v_m) for region-of-interest
- L1-distance of mini-batch $\mathbf{b}$:

$$\min_{\theta} \sum_{\mathbf{b}} \sum_{k=1}^{N} \gamma^{N-k} \cdot v_m \cdot \left\| \mathrm{f}_{gt}^{\mathbf{b}} - \mathrm{f}_{k}^{\mathbf{b}}(\theta) \right\|_1$$

Helmholtz-Zentrum hereon

VolRAFT

Synthetic 3D Displacement Field

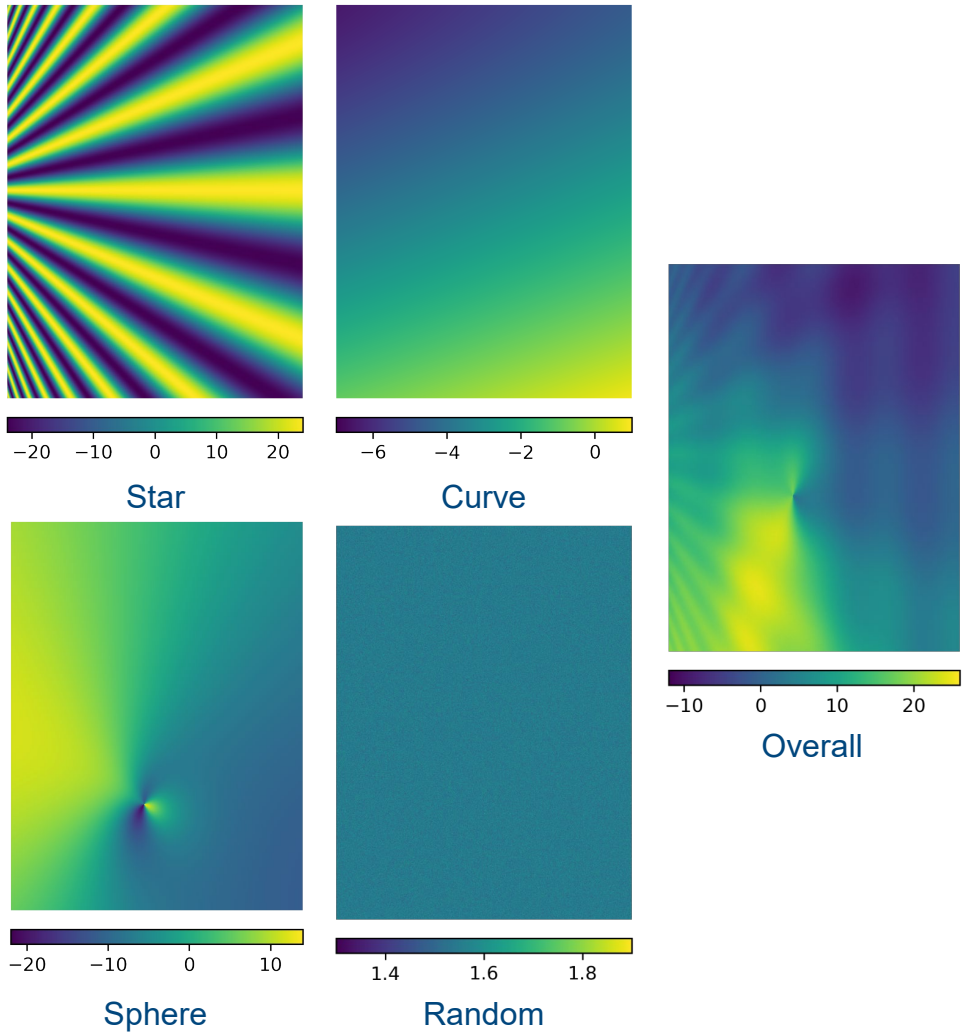

Real measured CT datasets (in total 39):

- Bone + Screw samples: Titanium (`Ti`), Magnesium Gadolinium alloy (`Mg-10Gd, Mg-5Gd`), Polyetheretherketone (`PEEK`)
- Denoised, Registration, Segmentation

Synthetic 3D displacement fields (in total 23):

- 4+1 classes: star, curve, sphere, random, overall
- Random data augmentation:
  - rotation by 3D angles, permutation of the axes order, addition of noise,
  - generation of random flow parameters, e.g.: amplitudes, spatial frequencies, non-linearity

Synthetic datasets (in total 897):

- 828 datasets for training and validation
- Exclude 3 samples (69 datasets) for testing the generalization: `PEEK_4w_5L, Mg-5Gd_4W_103L, Ti_4w_5R`

Helmholtz-Zentrum hereon

VolRAFT

Experimental Results: Synthetic Datasets

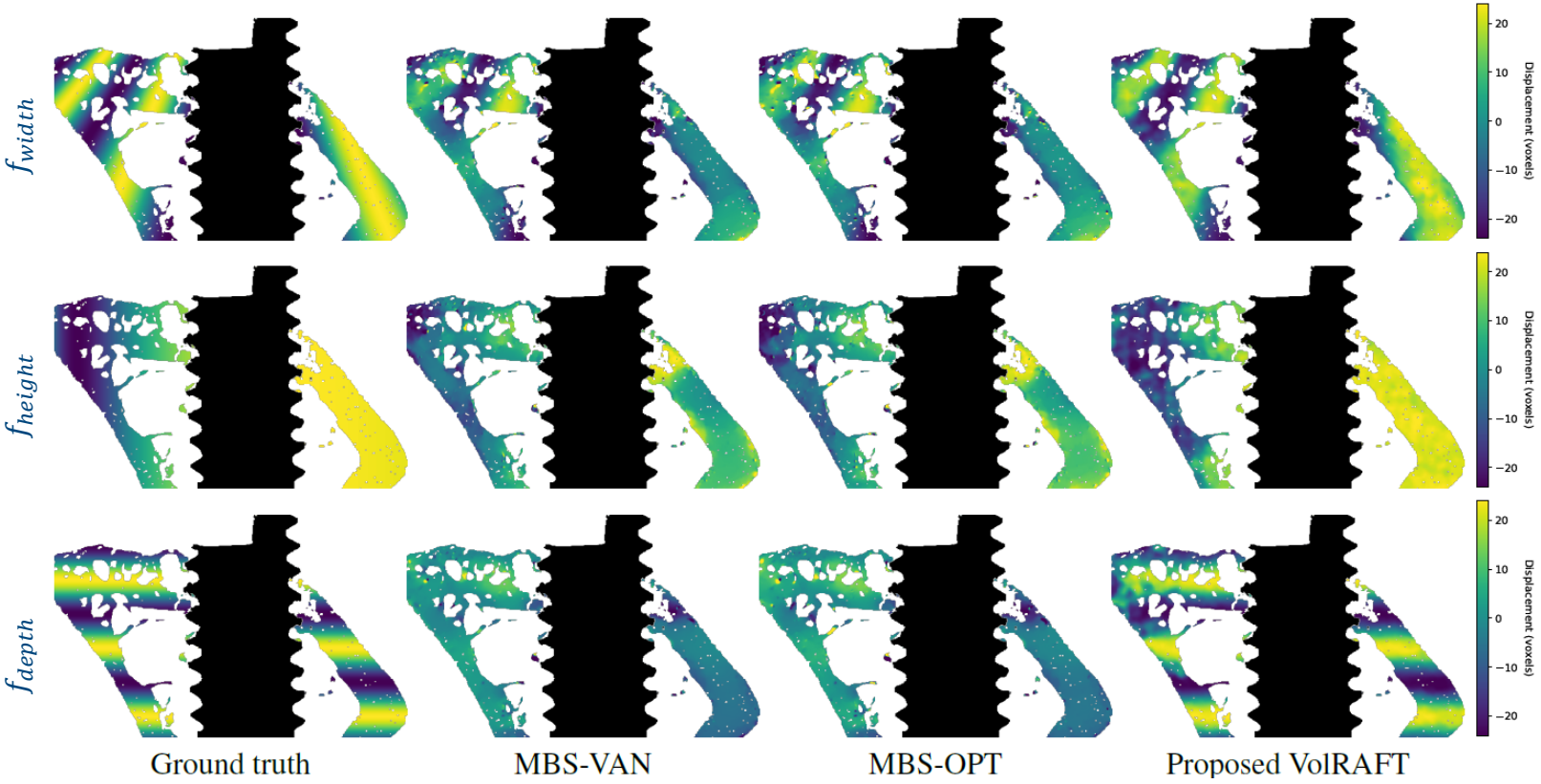

Sample	Disp. class	MBS-VAN	MBS-OPT	VolRAFT
PEEK_4w_5L	Star	20.686	24.406	**4.968**
PEEK_4w_5L	Curve	**0.680**	0.714	1.276
PEEK_4w_5L	Random	**0.187**	0.250	0.456
PEEK_4w_5L	Sphere	1.045	1.178	**0.880**
PEEK_4w_5L	Overall	1.195	1.406	**0.882**
*Mg-5Gd_4w_103L	*Star	20.526	20.136	**5.748**
Mg-5Gd_4w_103L	Curve	**0.356**	0.413	0.440
Mg-5Gd_4w_103L	Random	**0.140**	0.152	0.339
Mg-5Gd_4w_103L	Sphere	1.569	2.081	**0.855**
Mg-5Gd_4w_103L	Overall	1.149	1.280	**0.944**
Ti_4w_5R	Star	21.262	19.805	**4.426**
Ti_4w_5R	Curve	**0.923**	0.997	1.270
Ti_4w_5R	Random	0.313	**0.229**	0.307
Ti_4w_5R	Sphere	3.103	2.236	**1.078**
Ti_4w_5R	Overall	1.928	0.946	**0.706**

* MBS-OPT is empirically optimized by this dataset.

- VolRAFT generally resembles the Star displacement field
- However, VolRAFT can obtain block-based artifacts near the edge of homogeneous region due to patch-based inference methods

Comparison of End-Point-Error (EPE):

- Compare to iterative optical-flow-based DVC method (MBS-VAN)
- VolRAFT Generally performs better in displacement fields with strong and significant divergence and curl

Helmholtz-Zentrum hereon

VolRAFT

Experimental Results: Real Measurement Datasets

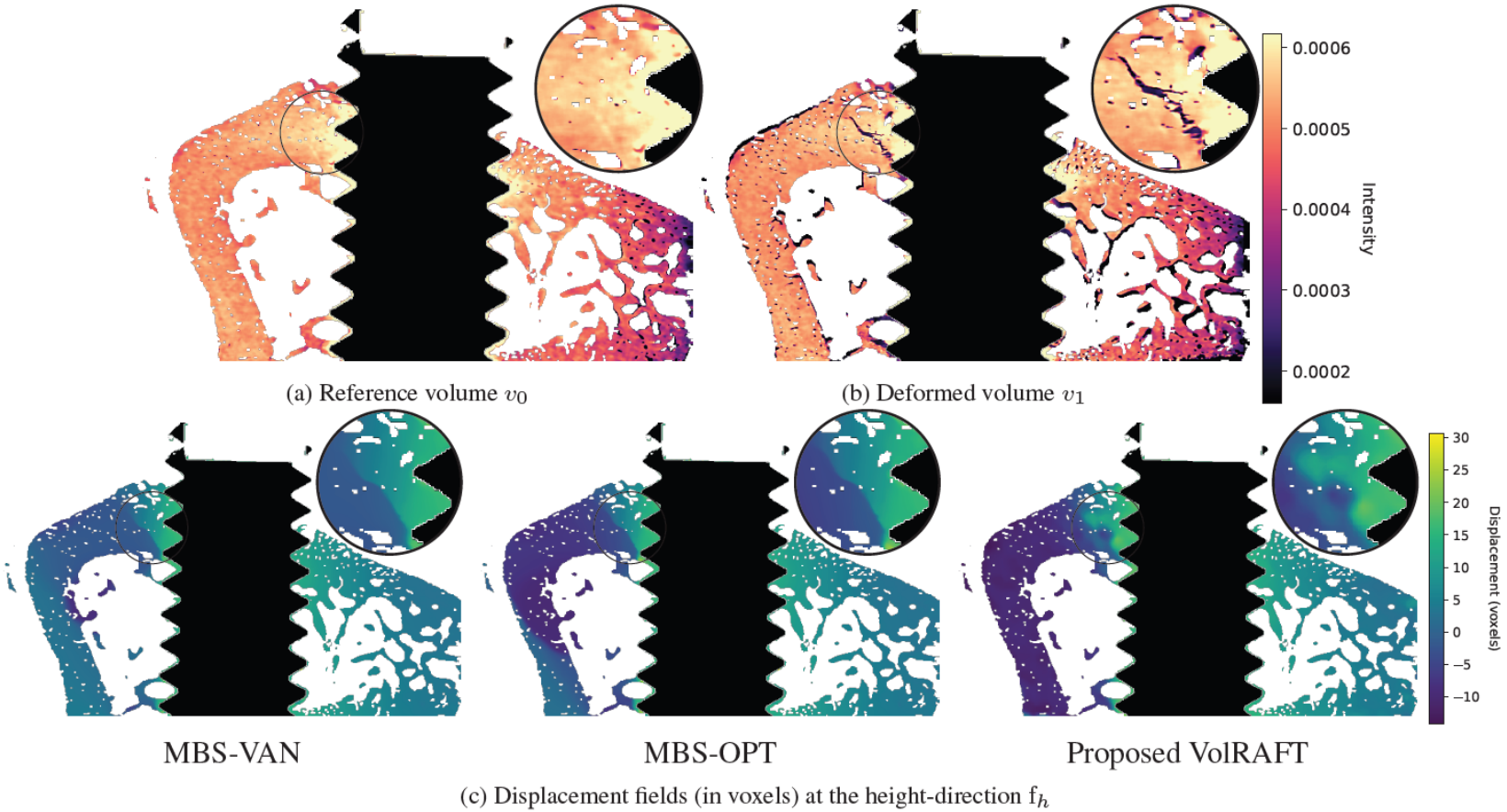

(a) Reference volume v_0 (b) Deformed volume v_1

(c) Displacement fields (in voxels) at the height-direction f_h

Real datasets by `Ti_4w_5R`:

- VolRAFT estimates the structure of displacement fields correctly
- Impressive generalization as samples are unknown in the training set
- Surprisingly, VolRAFT roughly estimate displacement for discontinuous and sharp structures in the fracture

Helmholtz-Zentrum hereon

VolRAFT: Volumetric Optical Flow Network for Digital Volume Correlation of SRμCT Images of Bone-Implant Interfaces

Summary

- Provides insight into application of SOTA computer vision approaches to address classical challenges in materials science research
- Can be improved by its inference method
- Can be potentially applied to other materials and experimental data
- Source code and trained network are available on GitHub: https://github.com/hereon-mbs/VolRAFT
- Paper accepted for oral presentation at IEEE / CVF Computer Vision and Pattern Recognition Conference Workshops (CVPRW), June 2024 – Computer Vision for Materials Science.

Acknowledgements

Hereon

- Stefan Bruns
- Diana Krüger
- Tamadur Adnan Albaraghtheh
- D.C. Florian Wieland
- Felix Beckmann
- Jörg Hammel
- Regine Willumeit-Römer

Ethics statement

The animal experiments were approved by the ethical committee at the Malmö/Lund regional board for animal research, Swedish Board of Agriculture (approval number DNR M 188-15). The authors declare no competing interests.

VolRAFT: Volumetric Optical Flow Network for Digital Volume Correlation of SRµCT Images of Bone-Implant Interfaces

Reference:

1. Tsakiris, Violeta, Christu Tardei, and Florentina Marilena Clicinschi. "Biodegradable Mg alloys for orthopedic implants–A review." Journal of Magnesium and Alloys 9.6 (2021): 1884-1905.
2. Lu, Yu, et al. "Biodegradable magnesium alloys for orthopaedic applications." Biomaterials translational 2.3 (2021): 214.
3. Krüger, Diana, et al. "High-resolution ex vivo analysis of the degradation and osseointegration of Mg-xGd implant screws in 3D." Bioactive Materials 13 (2022): 37-52.
4. Zeller-Plumhoff, Berit, et al. "Utilizing synchrotron radiation for the characterization of biodegradable magnesium alloys—from alloy development to the application as implant material." Advanced Engineering Materials 23.11 (2021): 2100197.
5. Bruns, Stefan, et al. "On the material dependency of peri-implant morphology and stability in healing bone." Bioactive Materials 28 (2023): 155-166.
6. Teed, Zachary, and Jia Deng. "RAFT: Recurrent All-Pairs Field Transforms for Optical Flow." European Conference on Computer Vision (ECCV). 2020.

Helmholtz-Zentrum hereon

Appendix

Further information

Helmholtz-Zentrum
hereon

Optical Flow

I_1 I_2

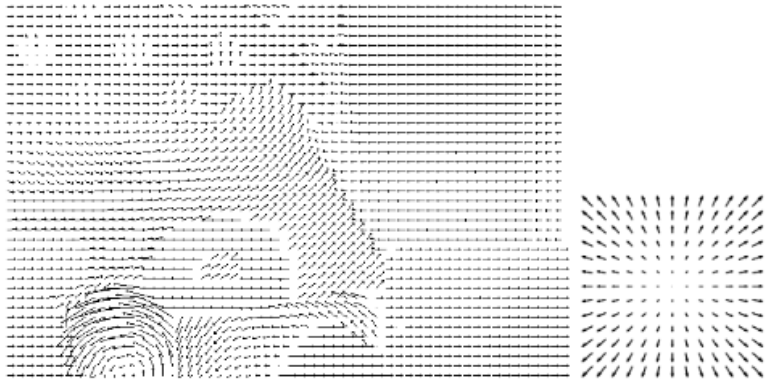

Arrow visualization

Optical flow represents motions/displacements of intensities in the image plane, but not necessarily accounts for the actual 3D motion in the physical scene.

Challenges: of classical iterative approaches:

- Classical iterative „Knowledge-driven approach“
  - Hand-crafting of hyperparameters: regularization, image pyramid, filtering, etc.
- Modern ML „data-driven approach“
  - Can outperform by learning the prior knowledge
  - Rely heavily on computing powers of GPUs, limited by GPU memory size

[5] Fortun, Denis, Patrick Bouthemy, and Charles Kervrann. "Optical flow modeling and computation: A survey." Computer Vision and Image Understanding 134 (2015): 1-21.

VolRAFT
Hyperparameter

Hyperparameter		RAFT-S	VolRAFT
Size of image/volume-patches		512×384	$\mathbf{80 \times 80 \times 60}$
Size of flow/displacement-patches		$2 \times 512 \times 384$	$\mathbf{3 \times 80 \times 80 \times 60}$
Optimizer		AdamW [21]	AdamW [21]
Learning rate		2e-5	2e-5
Number of epochs		100000	**10000**
Maximum range of displacement		400	**24**
(Mini-)Batch size **b**	Eq. (3)	6	**18**
Recurrent iterations N	Eq. (3)	12	12
Weights of loss γ	Eq. (3)	0.8	0.8
Levels of correlation matrix L		4	4
Gradient-norm clipped		$[-1, 1]$	$[-1, 1]$
Number of learnable parameters		1M	2.95M

Table 1. Comparison of hyperparameters and the number of learnable parameters between the RAFT-S model and our proposed VolRAFT approach. We take the default setting of hyperparameters from the source code of RAFT as a reference. The changed hyperparameters are highlighted.

VolRAFT
Training

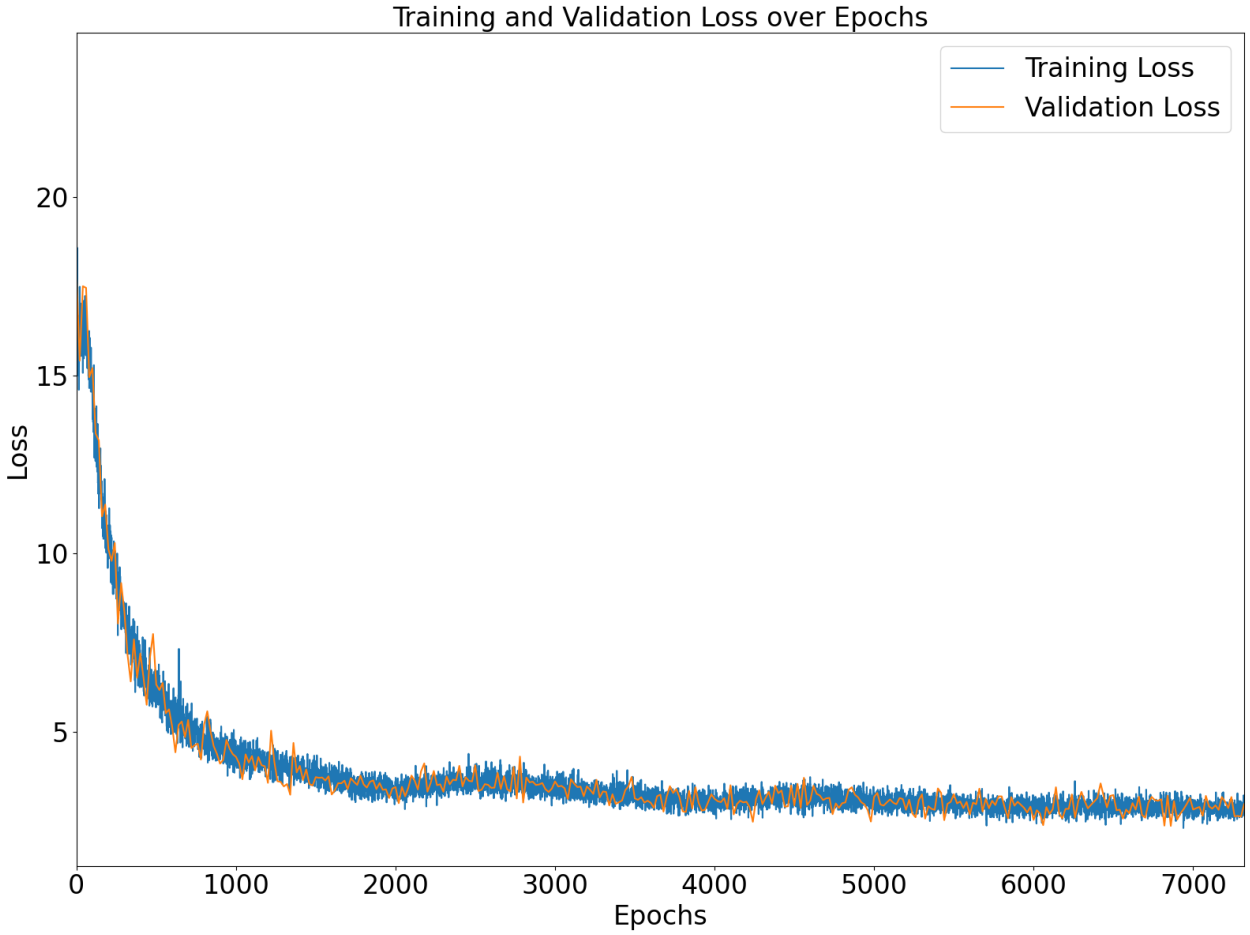

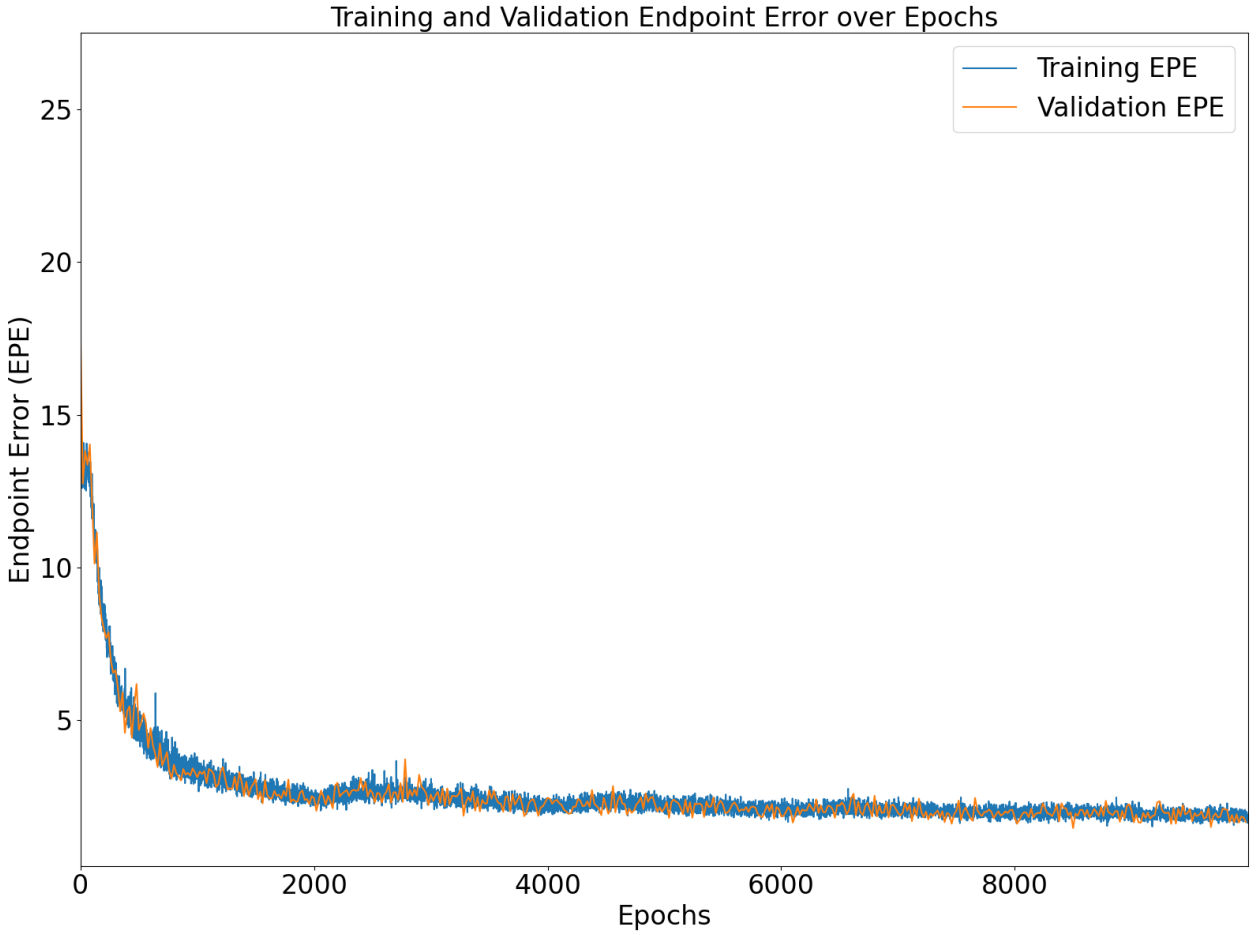

Helmholtz-Zentrum hereon

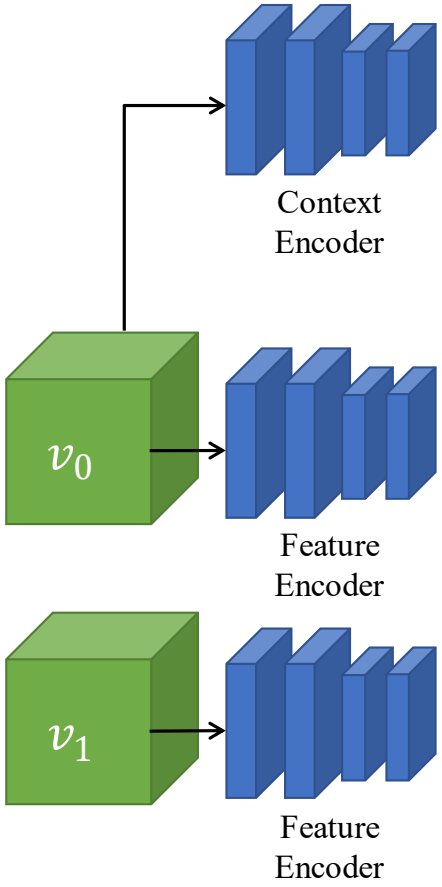

Patch-based approach:

- Splits full volumes (1280 x 1280 x 960) into patches (80 x 80 x 60) for training and inference

Feature/Context encoders:

- Convolutional layers
- Context and feature encoders are almost identical in their architectures

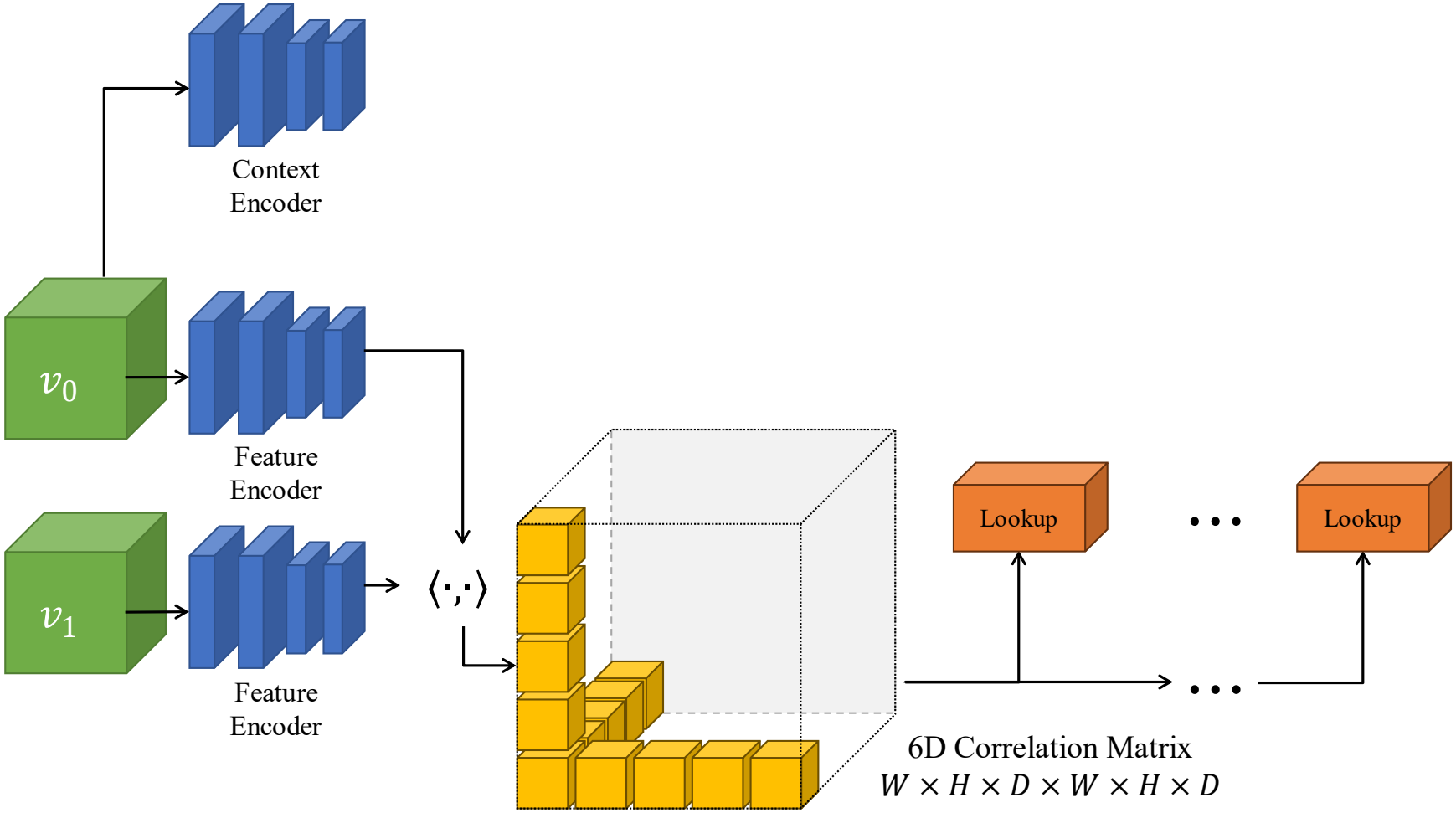

6D Correlation Matrix:

- Dot product to compute the similarity/correlation on multiscale pyramid
- Lookup operator to generate feature maps from correlation pyramid

Correlation Lookup Operators:

- Generate feature maps by indexing from correlation pyramid
- Grids around the projected spatial position on the deformed volume by trilinear sampling

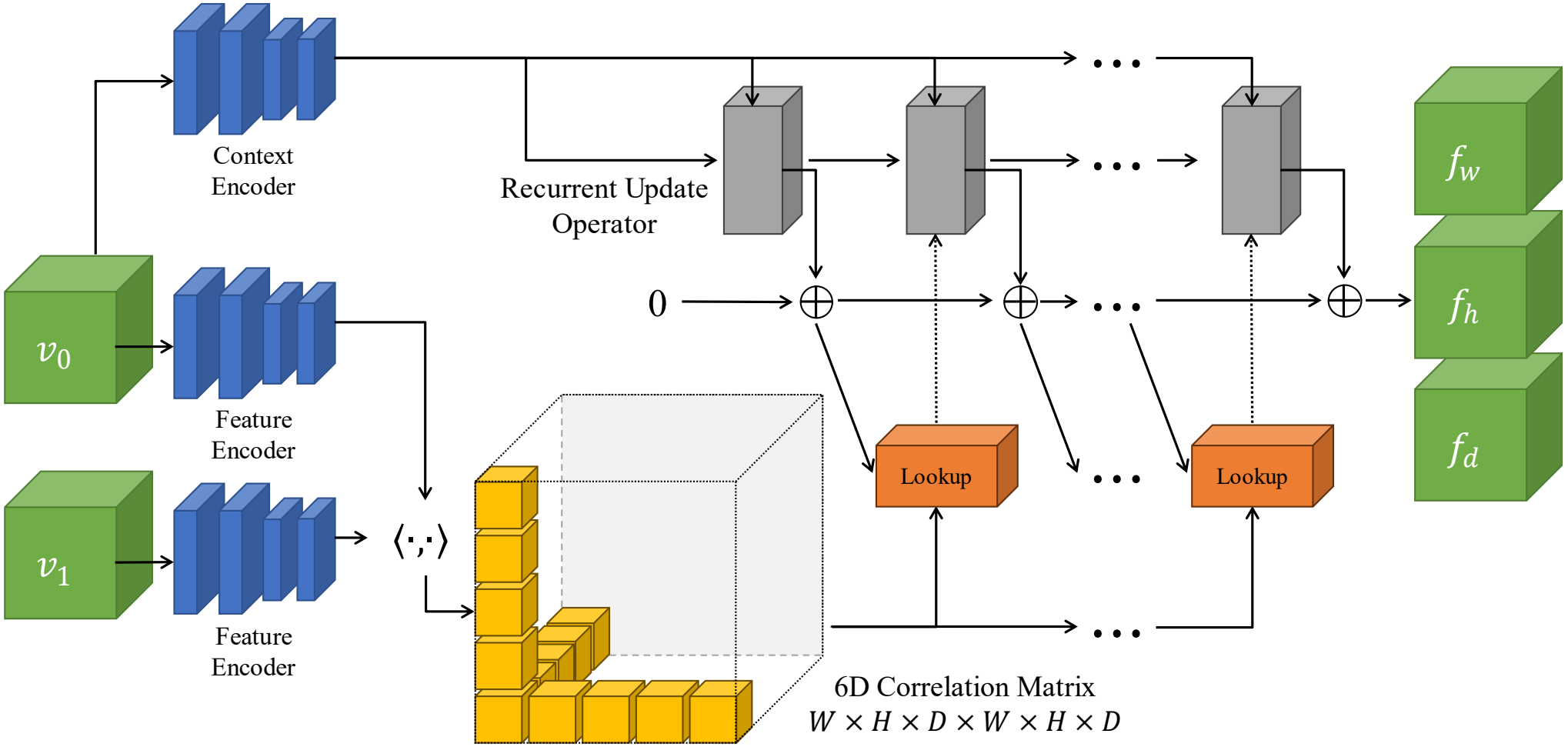

3D Recurrent Update Operator:

- Predict a sequence of displacement field
- Iteratively update by: correlation feature maps, previous displacement and context features

Supervised Loss with a foreground mask:

- Foreground segmentation mask (v_m) for region-of-interest
- L1-distance of mini-batch $\mathbf{b}$:

$$\min_{\theta} \sum_{\mathbf{b}} \sum_{k=1}^{N} \gamma^{N-k} \cdot v_m \cdot \left\| \mathrm{f}_{gt}^{\mathbf{b}} - \mathrm{f}_{k}^{\mathbf{b}}(\theta) \right\|_1$$

Helmholtz-Zentrum hereon